SUDDEN RELEASES OF HYDROGEN INTO A TUNNEL

Lyons, K.[1], Ewan, B., Rattigan, W.[1], Moodie, K.[1], Fletcher, J.[1], Moran, J.[1], Lang, T.[1], and Tremble, K.[1]

[1] Major Hazards, Science Division, Health and Safety Executive, Harpur Hill, Buxton, Derbyshire, SK17 9DZ, UK

Kieran.Lyons@hse.gov.uk; Wayne.Rattigan@hse.gov.uk; James.Fletcher@hse.gov.uk

ABSTRACT

This paper presents work undertaken by the HSE as part of the Hytunnel-CS project, a consortium investigating safety considerations for fuel cell hydrogen (FCH) vehicles in tunnels and similar confined spaces. The sudden failure of a pressurised hydrogen vessel was identified as a scenario of concern due to the severity of the consequences associated with such an event. In order to investigate this scenario experimentally, HSE designed a bespoke and reusable 'sudden release' vessel. This paper presents an overview of the vessel and the results of a series of 13 tests whereby hydrogen was released from the bespoke vessel into a tunnel at pressures up to 65 MPa. The starting pressure and the volume of hydrogen in the vessel were altered throughout the campaign. Four of the tests also included congestion in the tunnel. The tests reliably autoignited. Overpressure measurements and flame arrival times, measured with exposed-tip thermocouples, enabled analysis of the severity of the events. A high-pressure fast-acting pressure transducer in the body of the vessel showed the pressure decay in the vessel, which shows that 90% of the hydrogen was evacuated in between 1.8 and 3.2 ms (depending on the hydrogen inventory). Schlieren flow imagery was also used at the release point of the hydrogen, showing the progression of the shock front following initiation of the tests. An assessment of the footage shows an estimated initial velocity of Mach 3.9 at 0.4 m from the release point. Based on this, an ignition mechanism is proposed based upon the temperature behind the initial shock front.

1.0 INTRODUCTION

Hydrogen-powered vehicles are currently in service on UK roads [1] and have been demonstrated on the rail network [2]. There is the potential for further expansion in both road and rail usage, as well as other transportation technologies [3]. Due to the difference in behaviour between hydrogen and traditional fossil fuels, certain accident scenarios have different implications and potentially more severe outcomes when compounded by enclosed spaces such as tunnels. The HyTunnel-CS project [4] was created to identify and assess these scenarios [5]. The output of the project provides both theoretical and experimental insights into the identified scenarios, as well as recommendations for the safe use of hydrogen vehicles [6] and for updates to regulations, codes, and standards [7]. These insights and recommendations will enable more robust decision-making in the adoption of hydrogen vehicles.

One scenario identified was the catastrophic failure of a hydrogen vessel, whereby an onboard hydrogen storage pressure vessel (up to 70 MPa) bursts and releases the fuel very rapidly. HSE undertook a series of 13 experiments using a bespoke pressure vessel designed to provide repeatable rapid hydrogen releases. These experiments were conducted in a 70 m long, 3.7 m diameter steel tunnel at the HSE Science and Research Centre.

The objective was to understand the consequences of a sudden, catastrophic hydrogen release occurring in a tunnel. The effect of various hydrogen inventories, storage pressures, and congestion within the tunnel was also assessed.

2.0 METHODS

2.1 Experimental Facility

The facility used to complete the test campaign, which is described in more detail in the project deliverable report [8], consists of:

- hydrogen manifolded cylinder packs (MCPs) as the source of hydrogen;
- a two-stage boosting system that increases the pressure up to 70 MPa;
- the 70 m long, 3.7 m diameter steel tunnel;
- a hydrogen release mechanism, in this case the sudden release vessel;
- fast-acting pressure transducers and exposed-tip thermocouples;
- congestion structures in the tunnel.

Figure 1 shows a still taken from drone footage of the facility. The boosting facility is adjacent to the middle of the tunnel, which is where the hydrogen was released during the experiments. The fast-acting pressure transducers (indicated with triangles on the image) were installed into the sides of the wall to measure the blast overpressures and the thermocouple arrays (indicated with circles) were installed down the length of the tunnel. Table 1 and Table 2 show the sensor coordinates relative to the centre of the tunnel entrance at ground level (indicated with a square). The accuracy of the sensors is shown in Table 3. The congestion consisted of a set of 8 steel cuboids of 4.48 × 1.05 × 1.40 m arranged in two lines of 4 in the tunnel. A triangular sided wedge preceded each line of cuboids. These were approximately 4 m from the release point if they were present but had no impact on the observable results for the releases from the sudden release vessel so are not discussed further.

Figure 1: Overhead image showing the tunnel with sensor locations

Table 1: Blast pressure transducer locations.

Sensor ID	Co-ordinate (m)		
	x	***y***	***z***
P12	34.0	1.85	1.85
P11	36.0	1.85	1.85
P10	37.5	1.85	1.85
P9	40.0	1.85	1.85
P8	42.5	1.85	1.85
P7	45.0	1.85	1.85
P5	50.0	1.85	1.85
P3	55.0	1.85	1.85

Table 2: Thermocouple locations.

Sensor ID	Co-ordinate (m)		
	x	***y***	***z***
T45, T44, T43, T42, T41	34.0	0	3.25, 2.75, 2.15, 1.65, 0.95
T40, T39, T38, T37, T36	37.5	0	3.25, 2.75, 2.15, 1.65, 0.95
T35, T34, T33, T32, T31	40.0	0	3.25, 2.75, 2.15, 1.65, 0.95
T30, T29, T28, T27, T26	42.5	0	3.25, 2.75, 2.15, 1.65, 0.95
T25, T24, T23, T22, T21	45.0	0	3.25, 2.75, 2.15, 1.65, 0.95
T20, T19, T18, T17, T16	50.0	0	3.25, 2.75, 2.15, 1.65, 0.95
T15, T14, T13, T12, T11	55.0	0	3.25, 2.75, 2.15, 1.65, 0.95
T10, T09, T08, T07, T06	60.0	0	3.25, 2.75, 2.15, 1.65, 0.95
T05, T04, T03, T02, T01	65.0	0	3.25, 2.75, 2.15, 1.65, 0.95

Table 3: Sensor accuracies.

Instrument	Sensor	Make/model	Range	Accuracy
Pressure transducer (vessel)	P13	Kulite HKM-375-1000A	1000 PSI (abs)	± 0.5% FSO
Pressure transducer (blast)	P12, P11, P10	Kulite HKL-375M-100G	100 PSI (gauge)	± 0.5% FSO
Pressure transducer (blast)	P9, P8. P7, P5, P3	Kulite HEL-375-100A	100 PSI (abs)	± 0.5% FSO
Thermocouple	T01 to T45	Type K exposed tip	*n/a	*n/a

*n/a: the thermocouples were used as flame arrival detectors, not flame temperature sensors. The response time for these devices in approximately 0.003 s.

2.2 Sudden Release Vessel

The sudden release vessel is a bespoke pressure vessel designed to release its contents in a time frame similar to a bursting tank. This has been assessed to be in the order of 1.5 ms [9] [10]. This was achieved with a double bursting disk arrangement. Two 4" bursting disks with a bursting pressure of 40 MPa were arranged such that there were two separate compartments of the vessel: the main storage in the body, and the interspace in the top. The mode of operation was to pressurise these two chambers simultaneously but leave the interspace at 35 MPa. This resulted in the pressure difference across each bursting disk to be below the initiation pressure while allowing the main storage pressure to reach up to 70 MPa. The test was then initiated by venting the interspace, which increased the pressure difference across each bursting disc to greater than the burst pressure, releasing the hydrogen. Figure 2 shows a photograph of the vessel. Inserts were used to alter the internal volume of the vessel between 5, 12, and 18 liters. These volumes were scaled based on the unignited dispersion of a similar release in a full-scale tunnel [8]. Since these releases each ignited, the scaling method does not allow for extrapolation to real scenarios.

Figure 2: Image of the sudden release vessel

2.3 Schlieren Imagery

A release through the bursting disc will give rise to a spherical shock field. With the vessel exit pointing upwards, this means that a density discontinuity will be present in the vertical direction. To visualize (and potentially quantify) this effect, background oriented schlieren (BOS) [11] [12] was used. A black background plane of 2 × 1.5 m in size was covered with a white grid pattern 10 mm in width with 20 mm grid spacing. This was located against one wall of the tunnel, within which the vessel was located on the tunnel axis and pointing vertically upwards. The grid was illuminated with a 65000 lm constant light source inside the tunnel and imaged using a high-speed CCD camera, which was located outside the tunnel and using an 80 mm diameter viewing window. This is shown schematically in Figure 3.

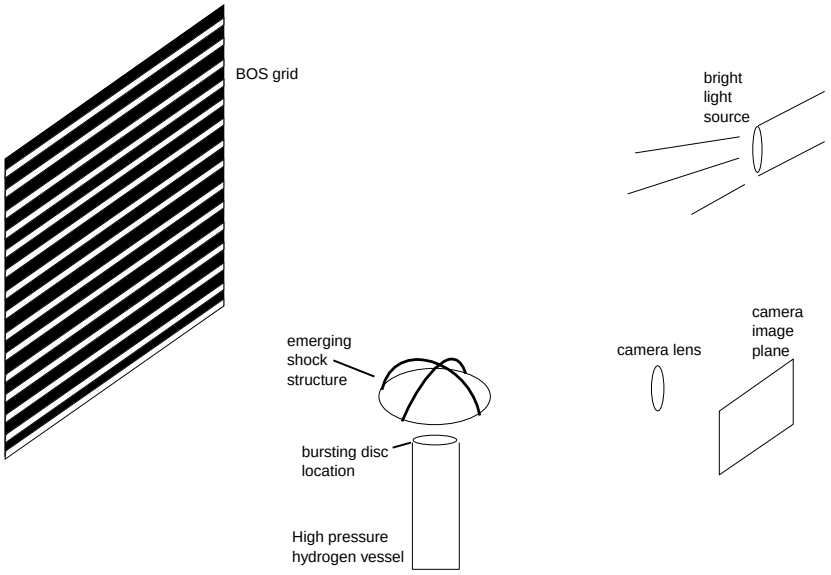

Figure 3: Sketch of the Schlieren setup

3.0 RESULTS AND DISCUSSION

Table 4 shows the initial conditions for each test in the experimental campaign, as well as a summary of the measured results. A larger volume and pressure typically resulted in higher measured overpressures, although variation was present between repeated initial conditions. The bulk of the results presented are from test 1, which is a representative case to demonstrate typical behaviour of the system.

Table 4: Experimental campaign summary results

Test No.	Initial Pressure (MPa)	Hydrogen volume (m^3)	Initial shock Mach No.	Initial overpressure at 0.4 m (kPa)	Peak overpressure at 1 m (kPa)	Peak overpressure at 20 m (kPa)
1	63.4	0.005	3.87	1762.6	89.7	42.1
2	63.4	0.005	3.60	1506.9	85.8	41.1
3	62.5	0.005	4.00	1870.4	84.5	34.3
4	66.0	0.012	*n/a	*n/a	101.5	49.7
5	65.8	0.012	3.65	1556.4	99.7	50.7
6	54.9	0.012	3.60	1506.9	93.9	43.5
7	60.2	0.012	3.83	1709.9	116.8	46.1
8	50.3	0.012	3.77	1657.9	90.6	45.5
9	61.2	0.018	4.00	1870.4	136.5	56.5
10	64.2	0.012	*n/a	*n/a	105.7	47.9
11	65.4	0.012	*n/a	*n/a	92.6	44.0
12	46.0	0.012	*n/a	*n/a	90.2	39.6
13	60.5	0.012	*n/a	*n/a	97.5	42.0

*n/a: the Schlieren was not in use during these tests.

3.1 Sudden release vessel evacuation

Figure 4 shows a graph taken from the pressure transducer in the sudden release vessel body from test 1, showing the pressure loss upon initiation. This is typical behaviour throughout the 13 tests.

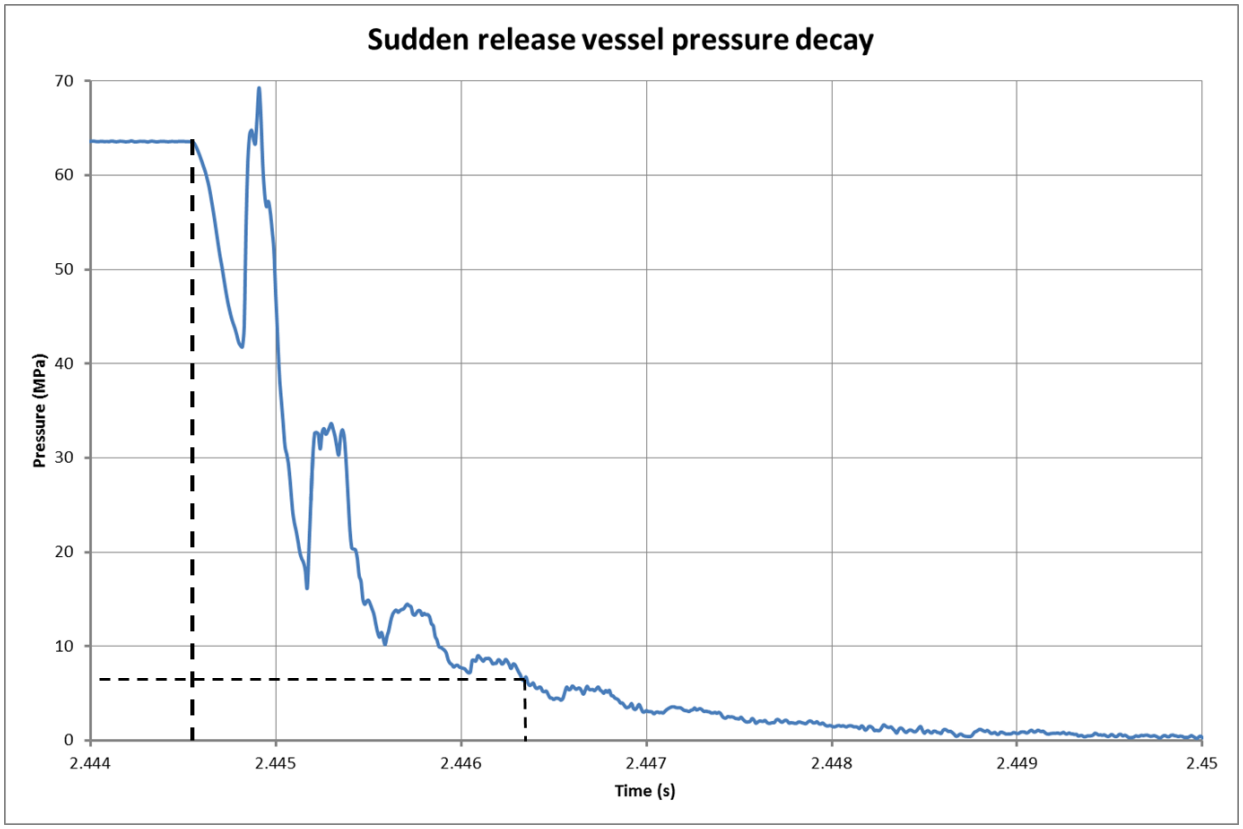

Figure 4: A graph of the pressure drop from the sudden release vessel after initiation

In this case, the pressure is initially maintained at just above 63 MPa, before the interspace is vented, which is highlighted on the graph. The pressure drops, then rises sharply. The time from the initial drop in pressure to the time 90% of the pressure has been lost in 1.8 ms. For 12 l cases, this increases to approximately 3.2 ms, and 5.2 ms for 18 l. This time compares favourably to the expected depressurisation time in a real tank burst scenario, suggesting that the sudden release vessel experiments are a reasonable representation. The pressure does not appear to be lost smoothly, with oscillations in the decay, including above the initial pressure. The cause of this behaviour is unclear, however a reaction force in the vessel upon initiation is possible.

3.2 Initial shock velocity

Immediately following the initiation of the release, a hemispherical shock wave emerged from the rupture site. The sequence of images such as those shown in Figure 5 have been recorded at 53 kHz. The position of the shock front, indicated with arrows on the images, has been plotted using the BOS grid as a calibrated background. This provides a semi-quantitative means of establishing the shock velocity as a function of distance from the disc position. The direct measurements of the shock moving up the backboard, counted as pixels, is then multiplied by a factor of 0.58 (based on the height of a nut measured against the backboard) to account for the perspective. The deceleration of the shock front is shown in Figure 6, which is the measured Mach number against the vertical distance from the release point for test 1. This is representative of the measurements made across each experiment.

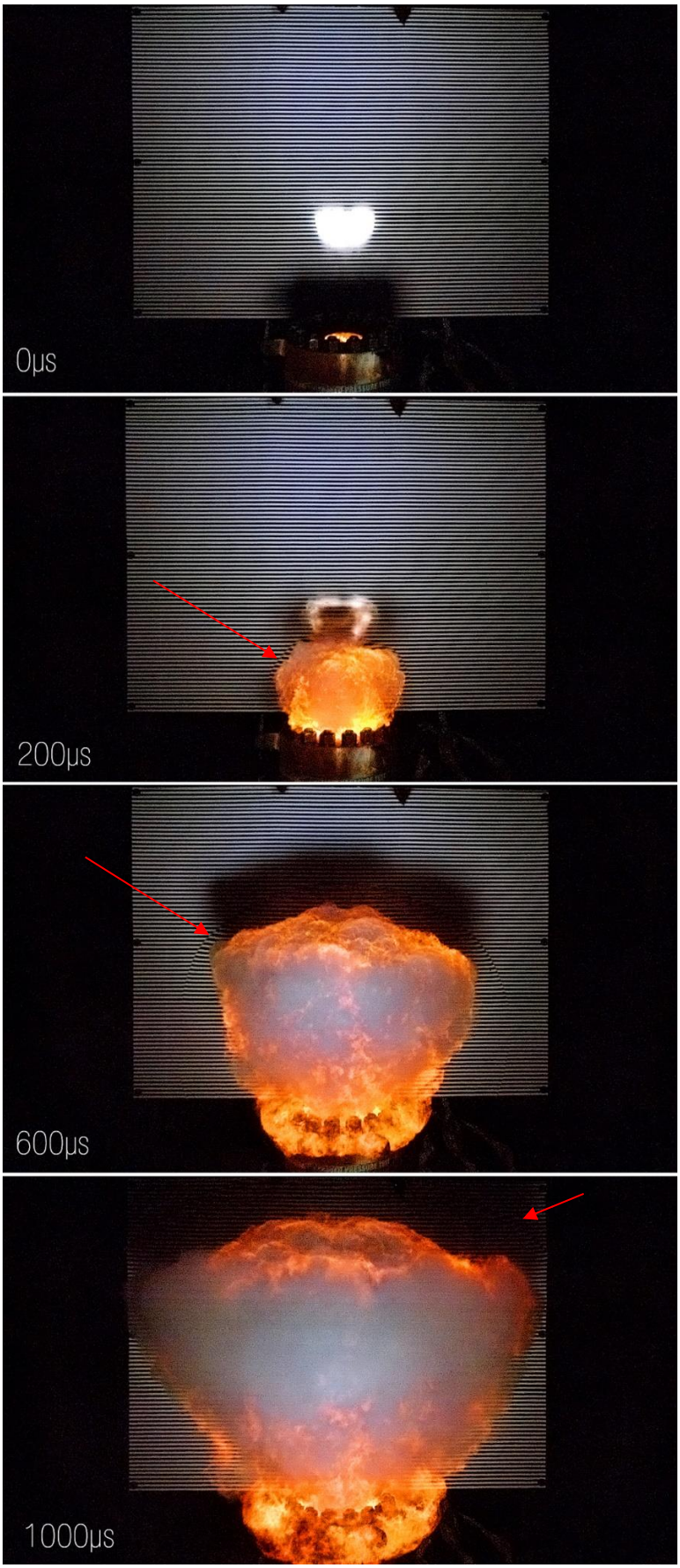

Figure 5: A series of stills showing the initial development of the shock

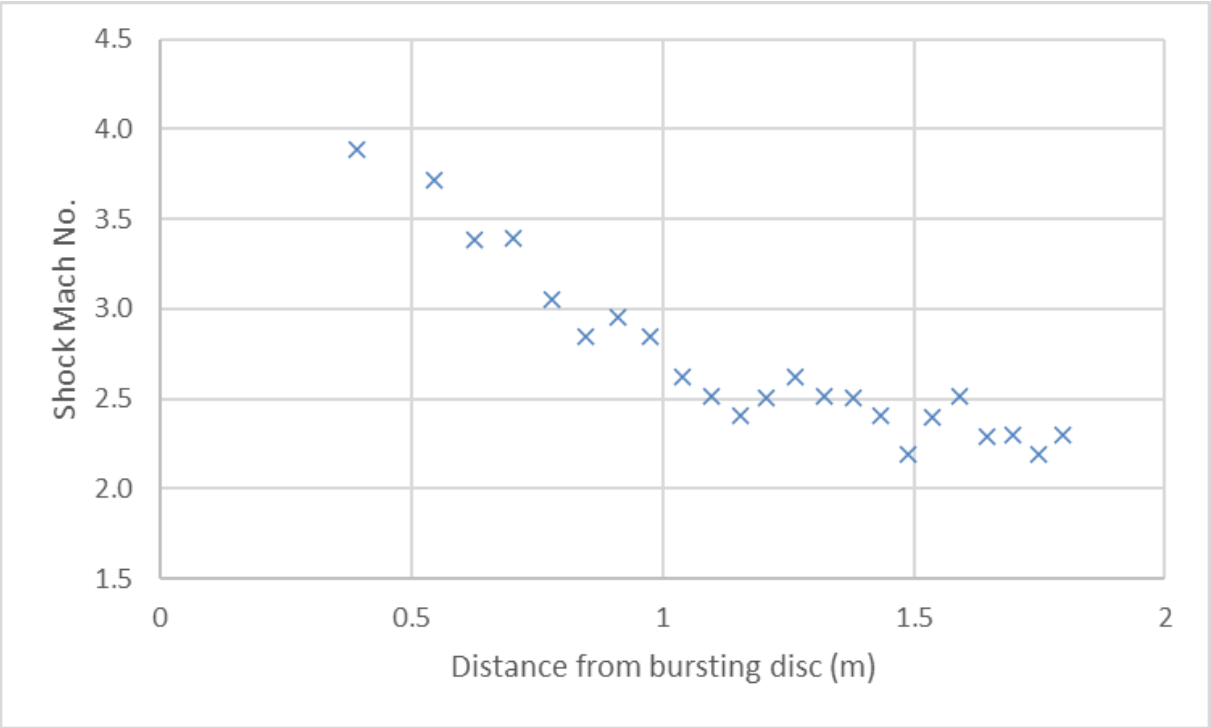

Figure 6: A graph of the measured shock speed using the Schlieren images from test 1

3.3 Ignition mechanism

Each test ignited without an external ignition source. From the high-speed footage, this appears to occur very quickly as luminescence is observable within the throat of the sudden release vessel in the first frame, as shown in Figure 5.

The proposed mechanism for this ignition relates to the initial shock velocity. Equation 1 [13] shows the relation between the Mach number of a shock and the temperature behind the shock assuming ideal gas behaviour. This allows for a prediction of the temperature based on the measured parameters in these experiments. The temperature was reliably calculated to be above 970 K.

$$\frac{T_2}{T_1} = \frac{[2\gamma M_1^2 - (\gamma - 1)]\,[(\gamma - 1)M_1^2 + 2]}{(\gamma + 1)^2 M_1^2} \quad (1)$$

These temperatures are reliably above the autoignition temperature for hydrogen. The hydrogen evacuates the vessel behind the shock, therefore encountering the turbulent and heated air that has been affected by the passing shock front. As this mixture reaches a flammable mixture, autoignition occurs due to the high temperature of the air. This mechanism was previously predicted by Maxwell and Radulescu [14].

While not visible in each recorded test, some evidence is present of secondary shock fronts developing during the events. Figure 7 shows a still from the Schlieren imagery potentially showing two distinct shock fronts. The proposed cause of this second front is the combustion of the highly turbulent hydrogen-air mixture. The second shock could also have a gas dynamic origin, however the shape of the raw overpressure measurements suggests a contribution to the pressure effects by a gas explosion.

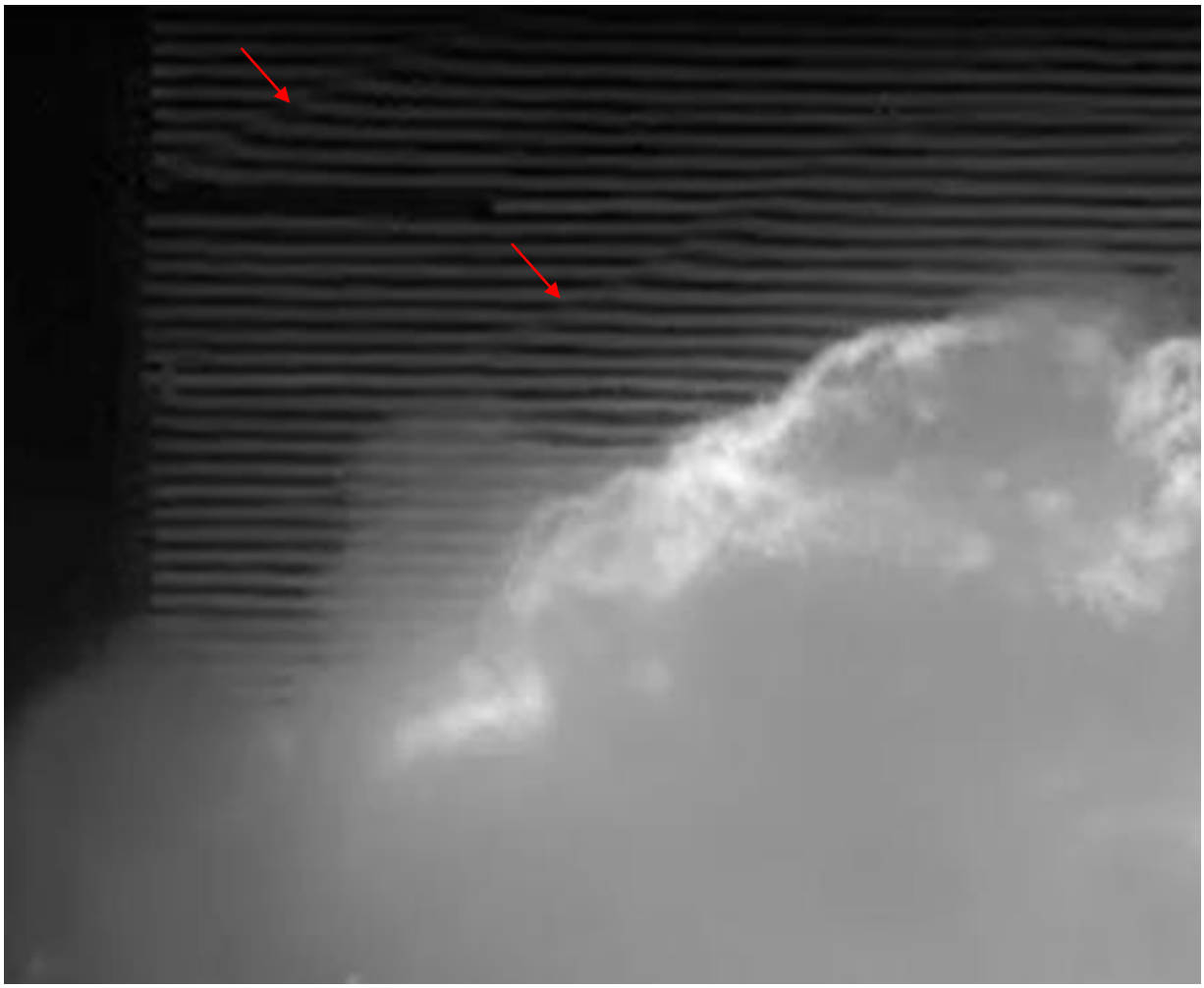

Figure 7: A still from the Schlieren imagery showing the presence of two pressure waves

3.4 Overpressure results

The overpressure results were obtained by two methods: calculation based on the measured shock velocity in the near field, and direct measurements using fast-acting piezo-resistive pressure transducers along the tunnel up to 20 m.

Using equation 2 [13], the pressure behind the shock can be calculated assuming ideal gas behaviour. The overpressure calculation in the near-field gives a pressure of approximately 1.8 MPa at 0.4 m from the release point, reducing to 0.6 MPa at 1.75 m. This is shown in Figure 8.

$$\frac{P_2}{P_1} = \frac{2\gamma M_1^2}{\gamma+1} - \frac{\gamma-1}{\gamma+1} \quad (2)$$

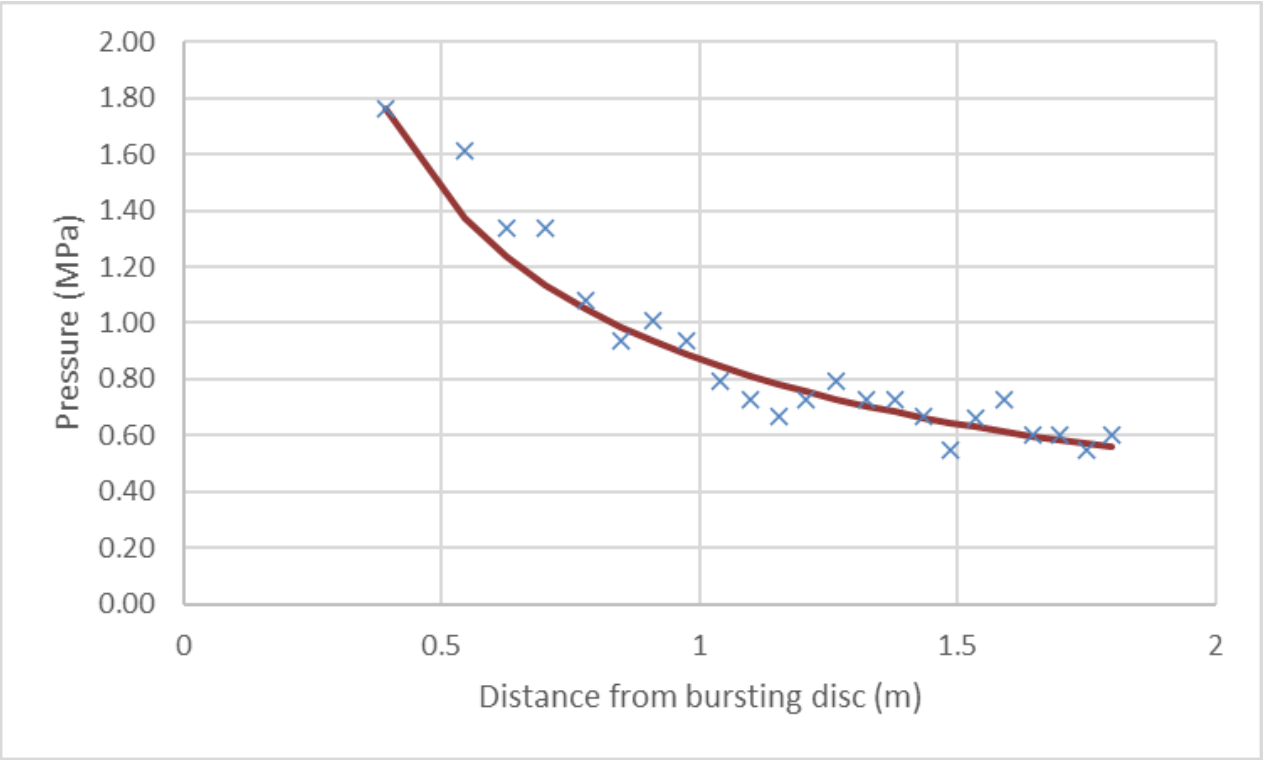

Figure 8: A graph of the calculated pressure of the shock near the release point for test 1

Using equation 3, an estimated best-fit curve is drawn through the data of Figure 8 taking the first data point as the reference P_o and radius r_o for the pressure P at radius r. Reported blast tests using small explosive charges [15] observe that the near field pressure decay can be represented in this form and where n was found to be 1.06. As can be seen the curve in Figure 8 is better represented using an n value of 0.9. The calculated values for these tests ranged between 0.7 - 1.0.

$$P = P_0 \left(\frac{r_0}{r}\right)^n \tag{3}$$

The initial pressure wave expands in three dimensions so follows typical decay curves, however as the pressure interacts with the steel tunnel, expansion in the lateral and vertical directions is stopped. This results in less attenuation than a free-field blast, with the primary decay in pressure caused by the tunnel roughness and rarefaction [16]. Overpressure measurements were made along the tunnel length at *x* distances between 1 m and 20 m from the release point. Since the wall of the tunnel is 1.85 m from the release point in the *y* direction, the closest pressure transducer is 2.1 m radially from the release point. This is greater than the radius of the tunnel, meaning each pressure transducer will measure the one-dimensional expansion mode of the blast wave.

Figure 9 shows the measured overpressures against the *x* distance from the release point. An approximation using equation 3 and an approximation using the 'saw-tooth' method described in a HSE Research Report [16].

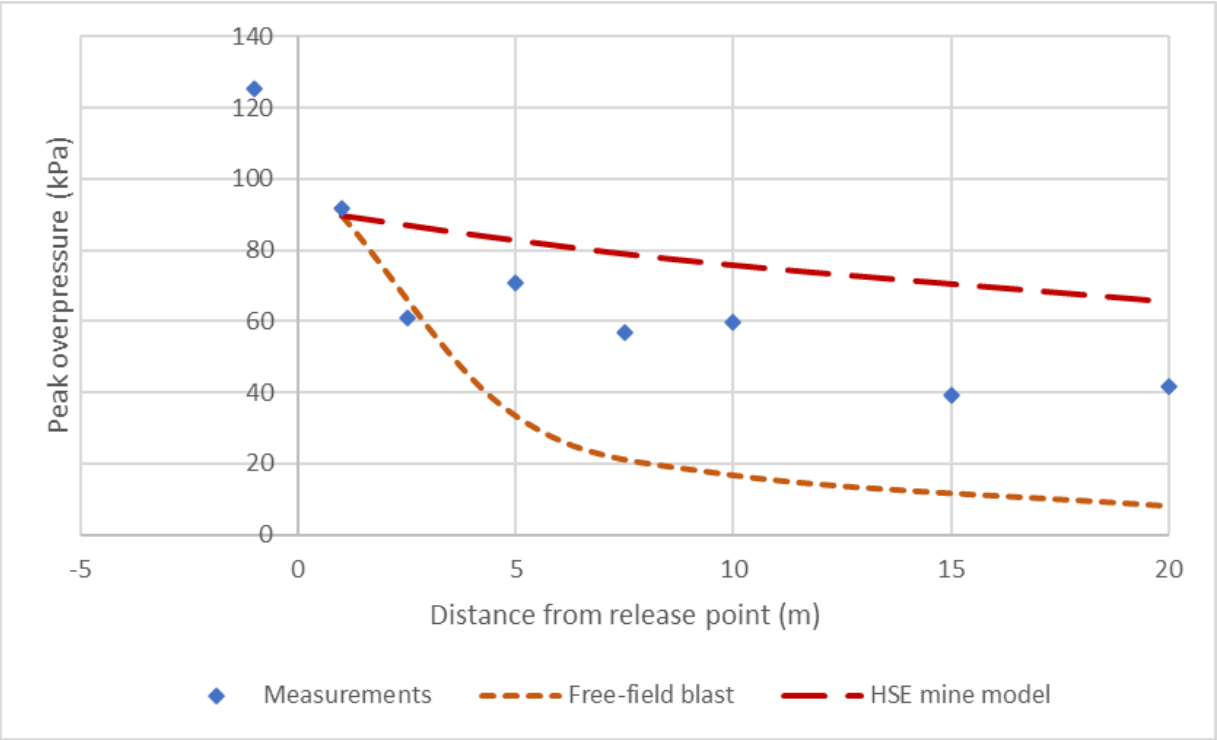

Figure 9: Peak overpressures from test 1 measured down the tunnel with approximations

The three-dimensional approximation underestimates the pressure at the end of the tunnel, whereas the HSE method is conservative in this case. This could be due to the relative smoothness and short length of the tunnel in this case, although it appears that the relative overestimation increases with distance. A potential cause of this could be the assumption in the model that the walls are rigid, whereas in reality some energy of the blast would be imparted onto the walls, inducing a flex and oscillations.

Another factor that could limit the effectiveness of the model is the difference in the type of explosion in a tank bursting event compared to condensed phase explosives. With both real tank ruptures and the sudden release vessel, there are two contributors to the blast effects: mechanical energy from the release of pressure, and chemical energy from the combustion [17] [18].

Figure 10 shows the raw output of the pressure transducers at 1, 10, and 20 m. These traces still contain the intrinsic noise of the sensors, reflections, and reverberations from the steel tunnel.

The nearest trace shows two distinct peaks. It is proposed that the first peak is the pressure developed from the mechanical energy of the bursting disc rupturing and the second peak is generated by the deflagration of the hydrogen. This is supported by the previous observation of secondary shocks being visible on the Schlieren imagery from Figure 7. As the front(s) move down the tunnel, the apparent behaviour of each is different. A qualitative assessment of the progression of the wave suggests that the initial peak moves slower and has greater attenuation than the second peak. This is shown in the set of graphs of Figure 10, which shows the pressure traces at various *x* distances down the tunnel.

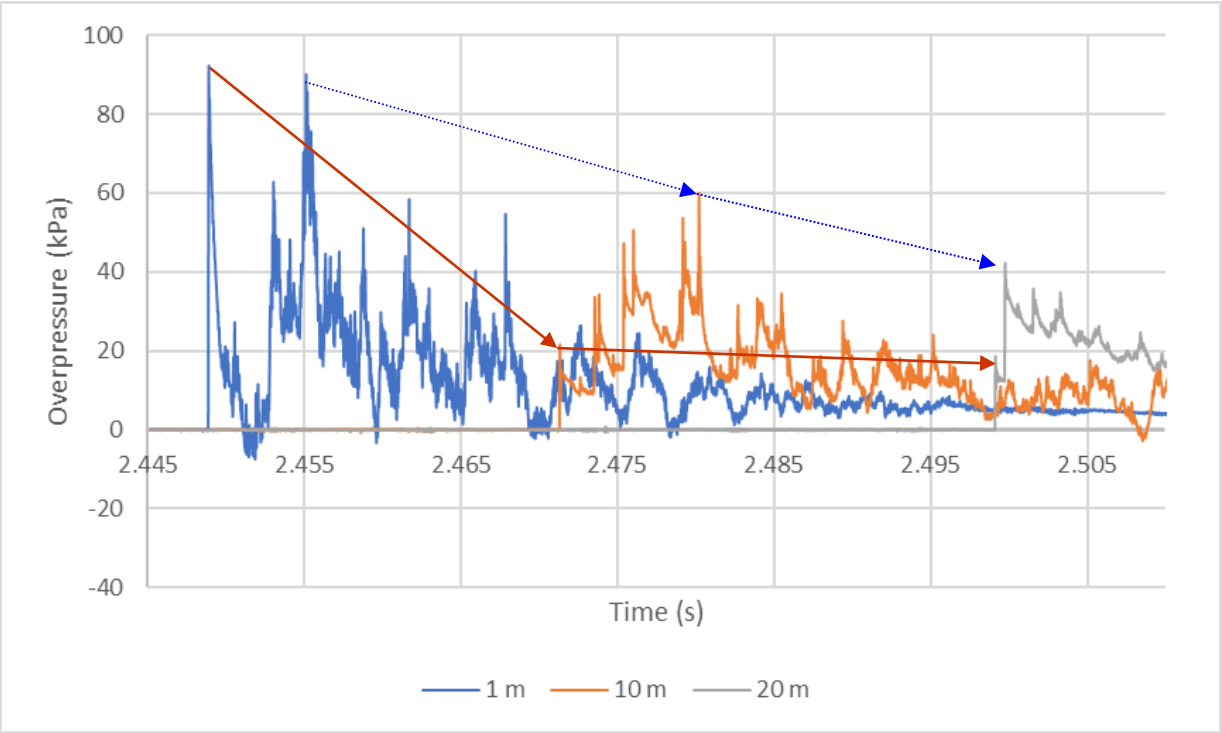

Figure 10: Raw overpressure traces taken at 1 m, 10, and 20 m down the tunnel for test 1

This effect is only observable relatively close to the event, as after the 20 m point the second peak appears likely to overtake or merge with the initial peak. The proposed mechanism of this is that the first shock front is moving into ambient air, and therefore induces higher thermal and kinetic energy. The second shock is then moving through the heated and turbulent air, so has a higher speed of sound and loses less energy to the air, reducing attenuation and causing a relative velocity between the two shocks. The second peak appears to undergo rarefaction as the primary attenuation mode, as evidenced by the alteration in the shape of the trace as it develops down the tunnel.

These observations have led to the following proposed description of the blast overpressure development in these cases, which may assist in the modelling of similar events:

- In the initial phase, the mechanical energy from the ruptured tank undergoes free-field expansion until the blast interacts with the tunnel walls.
- The deflagration of the tank inventory produces an independent shock front from the initial mechanical blast and follows shortly behind.
- From the point where the radius of the blast is equal to the tunnel diameter, the attenuation changes to a one-dimensional mode.
- As the two shocks progress down the tunnel, the attenuation is different for each peak due to the conditions of the air in which each shock is progressing.
- The difference in air conditions also causes a relative velocity between the shocks, leading to eventual merging to a single front.
- Presumably, the shock then undergoes attenuation in a similar mode to the initial shock in the one-dimensional mode. In these experiments, however, the tunnel was too short to observe this effect.

Based on the measured overpressure, the expected damage of these events [1913] [20] would be significant damage to structures and vehicles beyond 20 m, deaths in most humans up to 2 m radially, and universal injuries with widespread deaths beyond 20 m.

3.5 Flame speed down the tunnel

The thermocouple arrays provide a basis for assessing flame arrival times as the distance between each array is known, and the exposed tip means the sensors respond quickly to flame or hot gases. Flame progress speeds in the immediate vicinity of the vessel are in the range of 10 – 20 m/s to the 40 m distance. By the 50 m distance these have dropped to 1 – 3 m/s and continue at this level up to the tunnel exit. Total times for hot gases to be observed at the exit are typically 12 seconds. This is much lower than the expected times for the flame of a fast deflagration, suggesting that the combustion is a localised event around the rupture vessel and the subsequent expansion and convection of hot gas accounts for its transport at low velocities to the tunnel exit. Tests 10 to 13 had congestion present in the tunnel, which appeared to have little effect on the propagation of the event. This is likely to be caused by the combustion event being localized.

4.0 CONCLUSION

In summary, a series of 13 experiments were conducted whereby hydrogen was released at pressures up to 65 MPa from a bespoke sudden release vessel. The releases from this vessel resulted in short (approximately 1.5 ms) deprssurisation times for the hydrogen and displayed hemispherical shock fronts. This suggests that the experiments are a reasonable representation of a real tank rupture event.

In each experiment, the hydrogen ignited without an external ignition source. The proposed mechanism for this ignition is the heat imparted on the air from the initial shockwave. As the hydrogen then mixes with this hot air (calculated to be above 970 K at 0.4 m), ignition occurs. The pressure response from these events (the initial shock from the bursting disc then the deflagration of hydrogen) shows a characteristic double peak in the relative near-field. This could be understood to be a mechanical blast followed by a deflagration.

The peak overpressures were measured at approximately 85 to 135 kPa at 1 m, reducing to 35 to 50 kPa at 20 m. Throughout the tunnel this would result in widespread deaths and severe damage to structures and vehicles. Clearly, the rupture of a hydrogen tank is a situation to be avoided in a populated tunnel or confined space and should therefore be considered in the design of hydrogen vehicles.

As the pressure waves propagate down the tunnel, the attenuation is reduced by the restricted expansion of the pressure waves in the vertical and lateral direction by the tunnel walls. Various correlations have been compared to the measured results, which confirm a reduced attenuation compared to free-field blasts.

An assessment of the flame arrival times suggests that the combustion is a relatively localised event, resulting in the obstacles not impacting the severity measured.

The findings of this experimental campaign, as well as other practical, numerical, and theoretical studies have been combined to provide recommendations for the safe use of hydrogen and for updates to regulations, codes, and standards.

ACKNOWLEDGEMENTS

This project has received funding from the Fuel Cells and Hydrogen 2 Joint Undertaking (now Clean Hydrogen Partnership) under Grant Agreement No. 826193. The contents, including any opinions and/or conclusions expressed, are those of the authors alone and do not necessarily reflect HSE policy.

REFERENCES

1. Element Energy Ltd, “London: a capital for hydrogen and fuel cell technologies”, Hydrogen London, 2016.
2. C. Calvert, J. Allan, P. Amor, S. Hillmansen, C. Roberts, and P. Weston, “Concept development and testing of the UK’s first hydrogen-hybrid train (HydroFLEX)”, *Rail. Eng. Sci.*, vol. 29, pp. 248-257, 2021.
3. Department for Business, Energy & Industrial Strategy, “UK hydrogen strategy”, CP 475, 2021.
4. HyTunnel, “About HyTunnel-CS”, hytunnel.net. https://hytunnel.net/?page_id=31 (accessed Mar. 2023)
5. M. Pursell, M. Garcia, V. Molkov, T Van Esbroeck, and K. Vågsæther, “Report on selection and prioritisation of scenarios”, HyTunnel-CS, Rep. D1.3, 2019.
6. J.L. Saw *et al.* “Recommendations for inherently safer use of hydrogen vehicles in underground traffic systems”, HyTunnel-CS, Rep. D6.9, 2022.
7. J. van den Berg *et al.* “Recommendations for RCS”, HyTunnel-CS, Rep. D6.10, 2022.
8. W. Rattigan *et al.* "Results of the deferred experimental programme and associated activities", HyTunnel-CS, Rep. D4.4, 2022.
9. R. Zalosh and N. Weyandt, “Hydrogen fuel tank, fire exposure burst test”, SAE Technical Paper, 2005-01-1886, 2005.
10. J.Y. Zheng and P.F. Lui, “Elasto-plastic stress analysis and burst strength evaluation of AL-carbin fibre/epoxy composite cylindrical laminates”, *Computational Mater. Sci.*, vol. 42, pp. 453-461, 2008.
11. E. Goldhahn and J. Seume, “The background oriented schlieren technique: sensitivity, accuracy, resolution and application to a three-dimensional density field”, *Experiments in Fluids*, vol. 43, pp. 241-249, 2007.
12. M. Raffel, “Background-oriented schlieren (BOS) techniques”, *Experiments in Fluids*, vol. 56, pp. 1-17, 2015.
13. Ames Research Staff, “Equations Tables and Charts for Compressible Flow”, NACA, Rep. 1135, 1951.
14. B.M. Maxwell and M.I. Radulescu, “Ignition limits of rapidly expanding diffusion layers: Application to unsteady hydrogen jets”, *Combustion and Flame*, vol. 158, pp. 1946-1959, 2011.
15. M. Kandula and R. Freeman, “On the interaction and coalescence of spherical blast waves”, *Shock Waves*, vol. 18, pp. 21-33, 2008.
16. S. Coldrick and G. Atkinson, “Underground storage of explosives in mines: modelling blast effects”, HSE Research Report, RR1175, 2023.
17. V.V. Molkov, D.M.C. Cirrone, V.V Shentsov, W. Dery, W. Kim and D.V. Makarov, “Dynamics of blast wave and fireball after hydrogen tank rupture in a fire in the open atmosphere”, *Int. J. Hydrogen Energy*, vol. 46, pp. 4644-4665, 2021.
18. S. Kudriakov *et al.* “Full-scale tunnel experiments: blast wave and fireball evolution following hydrogen tank rupture”, *Int. J. Hydrogen Energy*, vol. 47, pp. 18911-18933, 2022.
19. R.K. Zipf and K.L. Cashdollar, “Explosions and refuge chambers. Effects of blast pressure on structures and the human body”, CDC, NIOSH-125. https://www.cdc.gov/niosh/docket/archive/pdfs/niosh-125/125-explosionsandrefugechambers.pdf (accessed Mar. 2023)
20. “Overpressure levels of concern”, Office of Response and Restoration, NOAA, response.rstoration.noaa.gov. https://response.restoration.noaa.gov/oil-and-chemical-spills/chemical-spills/resources/overpressure-levels-concern.html (accessed Mar. 2023)